HERMANSSON, K. (1985). *Acta Cryst.* B**41**, 161–169.
HERMANSSON, K., OLOVSSON, I. & LUNELL, S. (1984). *Theor. Chim. Acta*, **64**, 265–276.
HIRSHFELD, F. L. (1971). *Acta Cryst.* B**27**, 769–781.
HIRSHFELD, F. L. (1977). *Isr. J. Chem.* **16**, 226–229.
JOHNSON, C. K. (1976). *ORTEP*II. Report ORNL-5138. Oak Ridge National Laboratory, Tennessee, USA.
KELLERSOHN, T. (1992). *Acta Cryst.* C**48**, 776–779.
KELLERSOHN, T., DELAPLANE, R. G. & OLOVSSON, I. (1991). *Z. Naturforsch. Teil B*, **46**, 1635–1640.
LEHMANN, M. S. & LARSEN, F. K. (1974). *Acta Cryst.* A**30**, 580–584.
LUNDGREN, J. O. (1982). *Crystallographic Computer Programs.* Report UUIC-B13-04-05. Institute of Chemistry, Univ. of Uppsala, Sweden.
MCINTYRE, G. J., PTASIEWICZ-BAK, H. & OLOVSSON, I. (1990). *Acta Cryst.* B**46**, 27–39.
MASLEN, E. N., RIDOUT, S. C. & WATSON, K. J. (1988). *Acta Cryst.* B**44**, 96–101.
MASLEN, E. N. & SPADACCINI, N. (1989). *Acta Cryst.* B**45**, 45–52.
MASLEN, E. N., WATSON, K. J. & MOORE, F. H. (1988). *Acta Cryst.* B**44**, 102–107.
MENSCHING, L., VON NIESSEN, W., VALTAZANOS, P., RUEDENBERG, K. & SCHWARZ, W. H. E. (1989). *J. Am. Chem. Soc.* **111**, 6933–6941.
OLOVSSON, I. & JÖNSSON, P. G. (1976). *The Hydrogen Bond. Recent Developments in Theory and Experiments*, edited by P. SCHUSTER, G. ZUNDEL & C. SANDORFY, pp. 393–456. Amsterdam: North-Holland.
OLOVSSON, I., PTASIEWICZ-BAK, H. & MCINTYRE, G. J. (1993). *Z. Naturforsch. Teil A.* In the press.
PTASIEWICZ-BAK, H., MCINTYRE, G. J. & OLOVSSON, I. (1993). In preparation.
PTASIEWICZ-BAK, H., OLOVSSON, I. & MCINTYRE, G. J. (1993). *Acta Cryst.* B**49**, 192–201.
SAMSON, S., GOLDISH, E. & DICK, C. F. (1980). *J. Appl. Cryst.* **13**, 425–432.
SEARS, V. F. (1986). *Methods of Experimental Physics*, Vol. 23, *Neutron Scattering*, edited by K. SKÖLD & D. L. PRICE, pp. 521–550. New York: Academic Press.
THORNLEY, F. R. & NELMES, R. J. (1974). *Acta Cryst.* A**30**, 748–757.
WILKINSON, C., KHAMIS, H. W., STANSFIELD, R. F. D. & MCINTYRE, G. J. (1988). *J. Appl. Cryst.* **21**, 471–478.
ZALKIN, A., RUBEN, H. & TEMPLETON, D. H. (1962). *Acta Cryst.* **15**, 1219–1224.

Acta Cryst. (1993). B**49**, 192–201

Bonding Deformation and Superposition in the Electron Density of Tetragonal $NiSO_4.6H_2O$ at 25 K

BY H. PTASIEWICZ-BAK* AND I. OLOVSSON

Institute of Chemistry, University of Uppsala, Box 531, *S*-751 21 *Uppsala, Sweden*

G. J. MCINTYRE

Institut Laue–Langevin, BP 156, 38042 *Grenoble CEDEX* 9, *France*

(*Received* 12 *July* 1992; *accepted* 10 *September* 1992)

Abstract

The electron density in the title compound has been determined at 25 K by multipole refinement against single-crystal X-ray intensity data. Hydrogen positional and displacement parameters were fixed to values determined by refinement against single-crystal neutron data. The electron density based on the deformation functions of all atoms in the structure is compared with the individual densities calculated from the deformation functions of only nickel or the separate water molecules. In this way the effects of simple superposition of the individual densities have been studied. The individual deformation density around nickel is then in good qualitative agreement with that expected for an approximately octahedral $[Ni(H_2O)_6]^{2+}$ complex. The apparent decrease of the electron density in the lone-pair regions of the water oxygen atoms can be attributed to superposition of the oxygen density with the negative deformation density of nickel; the individual densities of the water molecules show clear polarization of the lone-pair densities according to the coordination of the water molecules. The individual densities of the water molecules are virtually identical with those earlier determined at room temperature. The densities around nickel show, however, clear differences: the heights of the outer negative lobes are increased, whereas those of the positive lobes are decreased as the temperature is raised from 25 K to room temperature. This is postulated to be due to a real change in the relative occupancy of the electronic energy levels. To the authors' knowledge this is the first time such an effect has been observed by diffraction methods. Crystal data: nickel sulfate hexahydrate, $NiSO_4.6H_2O$, $M_r = 262.86$, $P4_32_12$, $a = 6.7778$ (5), $c = 18.176$ (2) Å, $V = 834.98$ (2) Å^3, $Z = 4$, $T = 25$ K; λ(Mo $K\alpha$) = 0.71069 Å, μ =

* Permanent address: Institute of Nuclear Chemistry and Technology, Dorodna 16, 03-195 Warsaw, Poland.

0108-7681/93/020192-10$06.00

$2.553\ mm^{-1}$, $F(000) = 544$, $R(F) = 0.018$ for 2958 reflections (X-ray); $\lambda = 0.753$ Å, $\mu = 0.206\ mm^{-1}$, $R(F) = 0.058$ for 2156 reflections (neutron).

1. Introduction

The electron density of tetragonal $NiSO_4.6D_2O$ was studied earlier at room temperature by the present authors (McIntyre, Ptasiewicz-Bak & Olovsson, 1990). It was demonstrated that the true bonding deformation features of the water molecules and the nickel ion were to a large extent obscured by superposition of the densities of adjacent atoms/molecules. These superposition effects were studied by a simple but novel method, the use of partial model deformation maps, where only the fitted deformation functions centred on the respective water molecules or nickel ion were plotted.

Although the earlier diffraction data were collected at room temperature, the maps were of surprisingly good quality and even indicated deformation of the water molecules due to the surroundings, an effect which is normally considered to be too small to be detected experimentally. It is, however, important to repeat the same experiment at low temperature, as normally recommended for high-precision electron density work. Common wisdom also has it that bonding deformation is independent of temperature, provided there are no structural changes. As we shall demonstrate, however, this statement must be qualified for transition metals with partially occupied close-lying energy levels. The present study is based on X-ray and neutron data of tetragonal protonated $NiSO_4.6H_2O$ at 25 K. A general introduction and references to other structure studies of the title compound were given in our previous paper.

2. Experimental

X-ray data

Intensity data for the title compound were collected at 25 K from a nearly square bipyramidal crystal that exhibited the forms {001} and {101}, with dimensions 0.20 mm high and 0.40 mm along the base edges, volume $6.1 \times 10^{-3}\ mm^3$. The four-circle diffractometer was equipped with a (Huber) χ circle of diameter 400 mm and a two-stage closed-cycle helium refrigerator (Samson, Goldish & Dick, 1980). Graphite (002) monochromatized Mo $K\alpha$ radiation was used; cell dimensions were determined by least-squares fit to the θ values of 25 centred reflections. Reflections were scanned in the ω–2θ mode; in the range $1 \le \theta \le 15°$ all reflections with $k \ge 0$ were measured; in the range $15 < \theta \le 50°$ only reflections with h, k and $l \ge 0$ were measured; $(\sin\theta/\lambda)_{max} = 1.11$ Å^{-1}. In total 3992 reflections were measured, including repeated measurements of five standard reflections. Background corrections followed Lehmann & Larsen (1974), standard deviations estimated from counting statistics, Lorentz and polarization corrections applied; absorption correction by Gaussian integration using the calculated attenuation coefficient $\mu = 2.553\ mm^{-1}$, transmission range 0.65–0.68.

No time dependence of the intensities of the standard reflections was observed; the average instability constant for the five standard reflections was $\bar{P} = 0.77 \times 10^{-2}$. Averaging of the 3640 reflections for which $|F_o|^2 \ge 3\sigma(|F_o|^2)$ in the Laue group 422 gave 2958 unique reflections with an agreement index, $[\sum w(|F_o|^2 - \langle|F_o|^2\rangle)^2/\sum w|F_o|^4]^{1/2}$, of 0.028; here w is the inverse variance of the observed squared structure amplitude, $|F_o|^2$, and $\langle|F_o|^2\rangle$ is the average of $|F_o|^2$ for each set of equivalent reflections.

Neutron data

The crystal used for the neutron data collection was a 1.2 mm high truncated pyramid with a base 2.1×2.8 mm. The data were measured on the *D*9 four-circle diffractometer at the Institut Laue–Langevin, Grenoble, in a beam of wavelength 0.753 (1) Å obtained by reflection from a Cu (220) monochromator. The cell dimensions agreed with the X-ray determined values; a nearly complete set of unique reflections with $h \ge k$, $k \ge 0$ and $l \ge 0$ to $\sin\theta/\lambda = 1.02$ Å^{-1}, and a limited set of equivalent reflections with $l < 0$ was scanned, ω–$x\theta$ step scans (with x increasing from 1.0 at low θ to 2.0 at the highest θ); standard reflections measured at regular intervals showed no significant variation; the average instability constant was 0.023. Background corrections following Lehmann & Larsen (1974) and Lorentz corrections were applied; absorption correction was by Gaussian integration using an experimentally determined attenuation coefficient $\mu = 0.206\ mm^{-1}$ (C. Frost, personal communication); transmission range 0.634–0.808. Averaging of the 2617 scanned reflections in the Laue group 4/*mmm* gave 2168 unique reflections with an agreement index of 0.040.

All data-reduction programs and the full-matrix least-squares program *UPALS* used for structure refinement have been described by Lundgren (1982).

3. Refinements

The atomic positions from the previous room-temperature study of the deuterated compound (McIntyre *et al.*, 1990) were used as starting values in the refinements. In both the neutron and X-ray refinements the quantity minimized was $\sum w(|F_o|^2 - |F_c|^2)^2$, where $w^{-1} = \sigma^2_{count}(|F_o|^2) + k^2|F_o|^4$ and σ_{count} was derived from Poisson counting statistics. The constant k was fixed at 0.02 and 0.01 for the neutron

Table 1. *X-ray refinement details*

I, conventional refinement. VI, deformation refinement, *mm*2 symmetry assumed for the water atoms; water H atoms equivalent. VII, deformation refinement, water H atoms equivalent. $\Delta = |F_o|^2 - |F_c|^2$.

	I	VI	VII
n (number of reflections)	2958	2958	2958
p (number of parameters)	57	181	199
$R(F^2) = \Sigma\|\Delta\|/\Sigma F_o^2$	0.0355	0.0268	0.0266
$wR(F^2) = (\Sigma w\Delta^2/\Sigma wF_o^4)^{1/2}$	0.0579	0.0378	0.0374
$S = [\Sigma w\Delta^2/(n-p)]^{1/2}$	2.183	1.458	1.446
Number of reflections with $\Delta/\sigma > 4.0$	143	20	16

Table 2. *Fractional atomic coordinates and equivalent isotropic displacement parameters* (Å^2) *for* $NiSO_4.6H_2O$ *at* 25 K

Upper figures: neutron refinement; lower figures, when given: X-ray refinement VI. The form of the displacement factor is $\exp(-2\pi^2\Sigma_i\Sigma_j U_{ij}h_ih_ja_i^*a_j^*)$; $U_{eq} = (U_{11} + U_{22} + U_{33})/3$.

	x	y	z	U_{eq}
Ni	−0.21245 (6)	−0.21245 (6)	0.0	0.0027 (1)
	−0.21263 (2)	−0.21263 (2)	0.0	0.0034 (1)
S	−0.70911 (22)	−0.70911 (22)	0.0	0.0030 (2)
	−0.70930 (5)	−0.70930 (5)	0.0	0.0036 (1)
O(1)	−0.17388 (13)	0.04476 (13)	−0.05344 (5)	0.0068 (2)
	−0.17382 (10)	0.04447 (13)	−0.05339 (4)	0.0081 (2)
O(2)	−0.47243 (12)	−0.24605 (12)	−0.05701 (4)	0.0056 (1)
	−0.47239 (14)	−0.24597 (9)	−0.05710 (3)	0.0064 (2)
O(3)	−0.06757 (12)	−0.35978 (12)	−0.08493 (4)	0.0052 (1)
	−0.06753 (14)	−0.35981 (9)	−0.08595 (3)	0.0061 (2)
O(4)	−0.61859 (13)	−0.62248 (13)	−0.06655 (4)	0.0058 (1)
	−0.61859 (16)	−0.62253 (15)	−0.06657 (4)	0.0069 (2)
O(5)	−0.92505 (11)	−0.67288 (11)	−0.00159 (5)	0.0053 (1)
	−0.92513 (12)	−0.67304 (13)	−0.00160 (6)	0.0064 (2)
H(11)	−0.07780 (30)	0.14593 (30)	−0.04112 (12)	0.0206 (4)
H(12)	−0.25049 (34)	0.08165 (31)	−0.09621 (11)	0.0212 (5)
H(21)	−0.57037 (31)	−0.14552 (31)	−0.05730 (13)	0.0222 (5)
H(22)	−0.53606 (33)	−0.37582 (29)	−0.05963 (12)	0.0199 (4)
H(31)	0.01042 (31)	−0.46919 (29)	−0.06586 (12)	0.0202 (4)
H(32)	0.01639 (30)	−0.27539 (30)	−0.11639 (11)	0.0191 (4)

and X-ray data, respectively, based on the observed instability constants of the standard reflections.

Neutron data

The scattering lengths used were 1.0300, 0.2847, 0.5805 and -0.3741×10^{12} cm for Ni, S, O and H, respectively (Sears, 1986). Several extinction models within the Becker & Coppens (1974, 1975) formalism were tried; satisfactory agreement between the observed and calculated intensities of the low-angle data was obtained for an isotropic type-I model with Lorentzian mosaic spread. The maximum calculated reduction of intensity due to extinction was 0.28.

The 112 variable parameters were the scale factor, the angular mosaic width and the positional and anisotropic thermal parameters of all atoms. The agreement indices, as defined in Table 1, following the final refinement were $R(F^2) = 0.074$, $wR(F^2) = 0.080$ and $S = 1.21$. The final fractional atomic coordinates and equivalent isotropic displacement parameters are given in Table 2. The large values of R and wR reflect the extent of the data in $\sin\theta/\lambda$ and the low statistics in the weak high-angle reflections. The agreement is still considered to be satisfactory since S is very nearly 1.0 and there are only 38 reflections with $|\Delta/\sigma| > 3.0$ after the final refinement, with the constant k in the weighting scheme set to 0.02.

X-ray data

Only the 2958 reflections with $|F_o|^2 > 3\sigma(|F_o|^2)$ were used. Two sets of refinements were carried out: (*a*) a conventional refinement with the assumption of spherical atomic scattering factors and (*b*) deformation refinements in which the aspherical valence-electron distribution was fitted to multipole deformation functions. In both sets of refinements the spherical scattering factors for Ni, S and O were the neutral-atom relativistic Hartree–Fock scattering factors of Doyle & Turner (1968), while the non-relativistic Hartree–Fock scattering factor of Cromer & Mann (1968) was used for H. The anomalous-dispersion contributions were taken from Cromer & Liberman (1970). A number of extinction models within the Becker & Coppens (1974, 1975) formalism were tried. Again an isotropic type-I correction was found to be most appropriate. In all refinements the hydrogen positional parameters were fixed to the values refined from the neutron data.

(*a*) *Conventional refinement.* The following parameters were refined: the scale factor, the mosaic width and the positional and anisotropic displacement parameters of all atoms other than the H atoms. Initially, the hydrogen displacement parameters were fixed to the values refined from the neutron data.

Refinements were carried out in the enantiomorphic space groups $P4_12_12$ (x,y,z) and $P4_32_12$ $(\bar{x},\bar{y},\bar{z})$ where x,y,z are the coordinates given by Stadnicka, Glazer & Koralewski (1987) and $\bar{x},\bar{y},\bar{z}$ are the same coordinates with reversed signs. The two space groups correspond to the two possible senses of rotation of the screw axis. The significant imaginary anomalous-dispersion contributions allow the sense to be determined. Our crystal had clearly grown in the $P4_32_12$ enantiomorph [$wR(F^2) = 0.12$ in $P4_12_12$; $wR(F^2) = 0.058$ in $P4_32_12$], as was also the case for the deuterated compound. Stadnicka *et al.* (1987) and Angel & Finger (1988) also tested the agreement in the models $P4_12_12$ $(\bar{x},\bar{y},\bar{z})$ and $P4_32_12$ (x,y,z). These models correspond to reversal of the sense of the screw axis, with the structure of the motif and the atoms generated by the dyad axis left unchanged. Calculation of the interatomic distances shows that these models give physically unacceptable contacts between the layers along z, specifically an O···O contact of 2.19 Å between $Ni(H_2O)_6$ octahedra with an H···H contact of 1.76 Å. The possibility that $NiSO_4.6H_2O$ adopts either of these models can be

excluded. Because of the unphysical contacts that would arise at the domain boundaries it is also unlikely that twinning of the dextro- and laevo-rotatory forms will occur.

The X-ray refined coordinates for atoms other than H agreed satisfactorily with the neutron coordinates but the displacement parameters were systematically higher in the X-ray case. The average discrepancy for the O atoms was 12.5% (in the deuterated compound at room temperature the discrepancy was 38%). The hydrogen displacement parameters were therefore fixed to the neutron values multiplied by 1.125 in the final refinements. As can be seen from Table 1, the final agreement indices for the conventional refinement in $P4_32_12$ are reasonably small; however, Fourier difference syntheses calculated after this refinement showed clear residual features that should be amenable to modelling by a multipole expansion of the charge distribution of the valence electrons.

(*b*) *Deformation refinement.* To model the aspherical electron distributions, we used the multipole deformation functions proposed by Hirshfeld (1971) with modifications by Harel & Hirshfeld (1975) and Hirshfeld (1977). Details of the procedure were given in the previous paper. In that study, six series of deformation refinements were performed (numbered II–VII), with constraints that were successively relaxed. Based on experience from these refinements, only models VI and VII have been employed in the present study and for ease of comparison the same numbering will be used here. In model VI, *mm*2 symmetry is assumed for the water O atoms and the water H atoms are assumed to be equivalent. There was no significant improvement in agreement as the *mm*2 symmetry was relaxed (model VII; see Table 1) and we shall henceforth consider only the results of model VI, in accordance with the previous study. The positional and equivalent isotropic displacement parameters of the Ni, S and O atoms using this model are given in Table 2.* The final coordinates of the heavy atoms from the neutron and X-ray refinements agree within one e.s.d.

4. Results and discussion

The overall structure is described in earlier reports (Beevers & Lipson, 1932; Stadnicka *et al.*, 1987). The nickel ion is octahedrally coordinated by six water molecules. There are three crystallographically independent water molecules, which are bonded in quite different ways: water(1) is coordinated to nickel planar-trigonally, water(2) is coordinated to nickel in one of the 'lone-pair' directions but with no neighbour in the other tetrahedral direction, water(3) is coordinated to nickel in the same manner as water(2) but also accepts a hydrogen bond in the other tetrahedral direction. The water-bonding situation is illustrated in detail in Fig. 1 of our previous paper (McIntyre *et al.*, 1990). Selected bond lengths and angles derived from the neutron diffraction data of $NiSO_4.6H_2O$ at 25 K are given in Table 3. The foreshortenings of the S—O distances at room temperature (RT) compared with 25 K amount to 0.01 Å (~3 e.s.d.'s) and are most probably artifacts of larger anisotropic displacements of the O atoms at RT; indeed, application of a correction for riding motion reduces the foreshortenings to 0.004 Å. Similar differences are also observed in the geometry of the water molecules: the average O—H distance at 25 K is 0.976 Å, as compared with 0.968 Å at RT. The former distance is in close agreement with the average distance $r_g = 0.974$ Å in the vibrational ground state of the free water molecule (Kuchitsu &

Table 3. *Selected bond lengths* (Å) *and angles* (°) *for* $NiSO_4.6H_2O$ *at* 25 K (*neutron diffraction data*)

Standard deviations are given in parentheses. Superscripts on the atom symbols denote equivalent positions: (i) $y, x, -z$; (ii) $y, -1+x, -z$; (iii) $-1+x, y, z$; (iv) $-1+x, -1+y, z$; (v) $\frac{1}{2}-x, \frac{1}{2}+y, \frac{1}{4}-z$.

(*a*) Covalent bonds			
Ni—O(1)	2.013 (1)	O(1)—Ni—O(2)	87.94 (3)
Ni—O(2)	2.057 (1)	O(1)—Ni—O(3)	89.79 (3)
Ni—O(3)	2.084 (1)	O(1)—Ni—O(1')	90.45 (6)
		O(1)—Ni—O(3')	90.67 (4)
		O(2)—Ni—O(3)	88.67 (4)
		O(2)—Ni—O(2')	93.67 (5)
		O(2)—Ni—O(3')	90.85 (3)
		O(1)—Ni—O(2')	178.28 (4)
		O(3)—Ni—O(3')	179.35 (6)
S—O(4)	1.478 (1)	O(4)—S—O(5)	109.12 (5)
S—O(5)	1.484 (1)	O(4)—S—O(4')	109.88 (15)
		O(4)—S—O(5')	109.82 (5)
		O(5)—S—O(5')	109.06 (15)
(*b*) Water molecules			
O(1)—H(11)	0.972 (2)	H(11)—O(1)—H(12)	111.2 (2)
O(1)—H(12)	0.968 (2)		
O(2)—H(21)	0.967 (2)	H(21)—O(2)—H(22)	109.8 (2)
O(2)—H(22)	0.981 (2)		
O(3)—H(31)	0.974 (2)	H(31)—O(3)—H(32)	109.5 (2)
O(3)—H(32)	0.989 (2)		
(*c*) Hydrogen bonds			
O(1)···O(5^{iv})	2.719 (1)	O(1)—H(11)···O(5^{iv})	168.8 (2)
H(11)···O(5^{iv})	1.760 (2)		
O(1)···O(3^{v})	2.758 (1)	O(1)—H(12)···O(3^{v})	169.3 (2)
H(12)···O(3^{v})	1.801 (2)		
O(2)···O(5^{ii})	2.777 (1)	O(2)—H(21)···O(5^{ii})	154.6 (2)
H(21)···O(5^{ii})	1.872 (2)		
O(2)···O(4)	2.742 (1)	O(2)—H(22)···O(4)	172.3 (2)
H(22)···O(4)	1.767 (2)		
O(3)···O(5^{iii})	2.780 (1)	O(3)—H(31)···O(5^{iii})	156.3 (2)
H(31)···O(5^{iii})	1.861 (2)		
O(3)···O(4^{v})	2.718 (1)	O(3)—H(32)···O(4^{v})	167.6 (2)
H(32)···O(4^{v})	1.743 (2)		

* Tables of the observed and calculated structure factors and the anisotropic displacement parameters following the neutron refinement and the final X-ray deformation refinement have been deposited with the British Library Document Supply Centre as Supplementary Publication No. SUP 55660 (46 pp.). Copies may be obtained through The Technical Editor, International Union of Crystallography, 5 Abbey Square, Chester CH1 2HU, England.

Bartell, 1962). On the other hand, an elongation of 0.01–0.02 Å would be expected due to the hydrogen-bond interaction for an O···O distance of ~2.8 Å (Olovsson & Jönsson, 1976). The spread in the individual O—H distances at RT is somewhat larger than at 25 K. The difference between the distances at the two temperatures is, as expected, largest for the most foreshortened bonds. Thus, for example, O(1)—H(11) is 0.957 (3) Å at RT, as compared with 0.972 (2) Å at 25 K, whereas there is no significant difference in the longest bond O(3)—H(32): 0.986 (3) Å at 295 K and 0.989 (2) Å at 25 K. Isotope effects in the O—H distances on deuteration can be ignored.

A similar comparison between the O···O distances is more difficult as isotope effects may be substantial for hydrogen bonds. In some cases an isotope effect of 0.01–0.02 Å has been found for O···O distances of around 2.8 Å (measured at the same temperature; *cf.* Olovsson & Jönsson, 1976). The largest difference in the present case is +0.038 Å but it is impossible to judge whether this is mainly a temperature or an isotope effect.

A key premise in our comparison of the deformation densities at 25 K *versus* RT is that there is no remanent convolution in the static model maps of the density with the thermal displacement. This requires critical appraisal of the validity of the X-ray thermal displacement parameters. We have already noted that there are differences in the neutron and X-ray-determined parameters at RT and, to a lesser extent, at 25 K. If these differences are due to an uncorrected systematic effect, such as thermal diffuse scattering, which is absorbed entirely by the displacement parameters, the deconvolution is still complete.

Tests were also made on the internal vibrations of the SO_4 and H_2O molecules. Hirshfeld's (1976) rigid-body test (zero difference in the mean-square vibrational amplitudes along the vector between bonded nuclei of similar mass) is satisfied by S and its O atoms at both 25 K and RT. For water, a large difference in H (or D) and O amplitudes along the bond is expected due to the large mass difference and should be constant below 300 K. Our values [0.0058 $Å^2$ for H_2O at 25 K and 0.0056 $Å^2$ for D_2O at RT, in both cases averaged over the six H(D)—O distances] are lower than the averages observed for water molecules in other hydrates (Eriksson & Hermansson, 1983) but still larger than the theoretical values. This agreement also supports our scaling of the neutron H(D) displacement parameters for the X-ray refinements. We also observe amplitude differences acceptably close to zero for the pair of H atoms in each water molecule along their interatomic vector as expected if the bending vibration does not mix significantly with the rocking vibration (Eriksson & Hermansson, 1983). The out-of-(water)-plane vibration of the water O atom decreases both at 25 K and at RT in going from O(1) to O(2) to O(3), which is consistent with the change from trigonal to partial tetrahedral to full tetrahedral coordination of the water molecule; at both temperatures the out-of-plane mean-square amplitude of O(1) is twice that of the in-plane components, while for O(3) the amplitude is nearly isotropic.

Deformation electron densities

Some general arguments for the use of deformation model maps instead of $X-N$ maps were given in the previous paper. Furthermore, some advantages in the use of partial deformation maps were discussed, the most important being the possibility to eliminate effects due to superposition of the deformation functions of neighbouring atoms and to interpret bonding effects within the traditional hydrogen-bond partitioning scheme (*cf.* Yamabe & Morokuma, 1975).

The static multipole model deformation maps for the sections of interest around Ni and around the three water molecules after refinement VI are illustrated in Figs. 1 and 3, respectively. In the diagrams the three atoms defining each section are written without parentheses. For orientation purposes other atoms close to these sections and the relevant H atoms are indicated within parentheses. In an attempt to distinguish the characteristic features of the Ni ion and the water molecules, the maps calculated from only the deformation functions of each of these constituents are also plotted separately. The numbering of the maps is the same as in the previous paper and for a detailed comparison this paper should be consulted. Only a few of the RT results are repeated here to illustrate the most important points. The corresponding dynamic maps are very similar to the static ones and are therefore not shown here.

(*a*) *The* Ni *atom.* In both the total and partial deformation maps the positive peaks are much more pronounced at 25 K than at RT, whereas the outer negative peaks are slightly less well developed at 25 K (*cf.* Figs. 1*a* and 2*a*). The positive peaks are very similar in the total and partial maps. The outer negative peaks on the other hand are strongly reduced in the total deformation maps in comparison with the partial maps at both temperatures (*cf.* Figs. 1*a*, 1*a'* and 2*a*, 2*a'*). These outer negative peaks are directed towards the positive peaks of the water ligands and it is then not surprising that superposition will lead to strongly reduced outer negative peaks around Ni. The positive peaks, on the other hand, will not be affected as no ligands are attached in these directions. The overall features expected for an Ni^{2+} ion in an approximately octahedral crystal

field are well reproduced in the partial maps (see our previous paper). The electron deformation maps in other sections not shown here have the same features and similar effects due to superposition as just discussed. The observed differences between the RT and 25 K maps may be due to different occupation of the upper energy levels, the splitting of which is a result of deviations from an ideal octahedral environment (see below).

(*b*) *The water molecules*. The deformation densities are illustrated both in the planes of the water molecules and perpendicular to these, through the two-fold axes, both with all deformation functions included in the calculation (Figs. 3*a*–3*f*), and with only the deformation functions of oxygen and hydrogen of the water molecule in question included (Figs. 3*a*′–3*f*′). The general features of the densities in the O—H bonds and the lone-pair regions were discussed in the previous paper. For the water molecules, the differences between the total maps at RT and those at 25 K are much smaller than for nickel. The superposition effect, when comparing the total and partial maps, is very similar at the two temperatures (*cf.* Figs. 3*a*, 3*a*′ and 4*a*, 4*a*′). As discussed in some detail in the previous paper, the apparent decrease in the lone-pair density as water receives a hydrogen bond or is coordinated to a metal ion is clearly an artifact, caused by the superposition of the deformation features from its neighbours. This is also illustrated separately for the hydrogen bond O(1)—H(12)···O(3) in Fig. 5.

Mirror symmetry in and perpendicular to the plane of the water molecule was imposed in the refinement and this is evident in the individual defor-

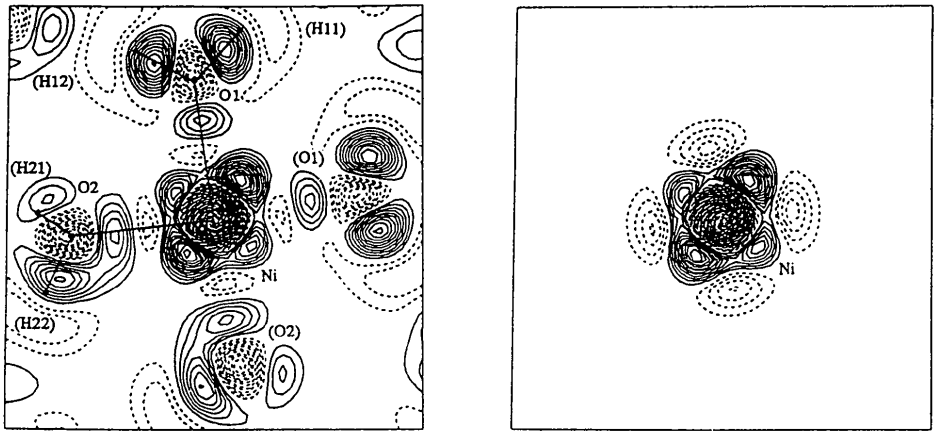

(*a*) (*a*′)

Fig. 1. $Ni(H_2O)_6$ static deformation model maps based on a full set of reflections to $\sin\theta/\lambda = 1.11$ Å^{-1}, calculated in the plane through Ni, O(1) and O(2). (All maps in Figs. 1–5 are based on refinement VI.) (*a*) All atoms are included in the calculation. (*a*′) Only the Ni deformation functions are included. Contours are drawn at intervals of 0.05 e Å^{-3}. Negative contours are dashed; the zero-level contour is omitted.

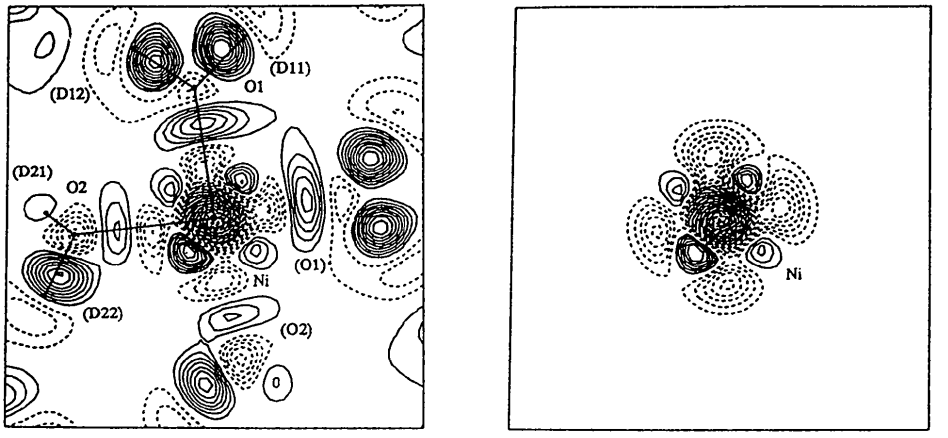

(*a*) (*a*′)

Fig. 2. Maps corresponding to Fig. 1, based on the RT study of $NiSO_4.6D_2O$ (McIntyre *et al.*, 1990). Approximations in previous Fourier calculations have been eliminated here and in Fig. 4; this has resulted in noticeable improvements compared to earlier maps (*loc. cit.*).

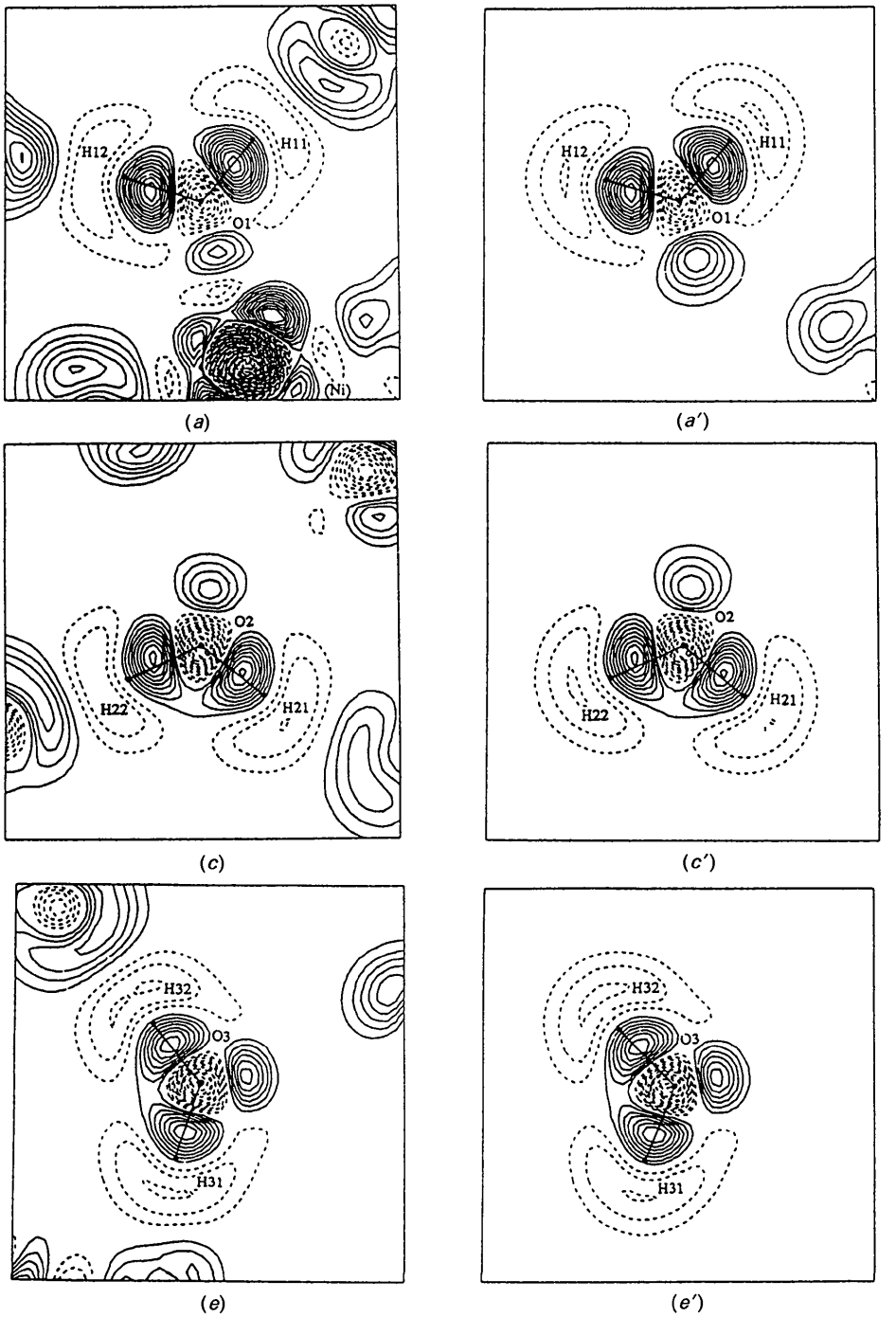

Fig. 3. (*a*), (*c*), (*e*) Static deformation model maps in the planes of the unique water molecules 1, 2, 3, respectively. All atoms are included in the calculation of the unprimed maps; only the deformation functions of the O and H atoms of the water molecule in question are included in the primed maps. Reflection limit and contours as in Fig. 1.

mation maps. Relaxing these constraints caused little change in the maps or in the agreement between observed and calculated structure factors (Table 2). It is beyond the accuracy of our data to attempt to interpret differences in the lone-pair lobes on a given water molecule.

Concluding remarks

The principal conclusions drawn from our earlier room-temperature study of $NiSO_4.6D_2O$ also hold for $NiSO_4.6H_2O$ at 25 K. Plots of model maps, calculated from only the deformation functions

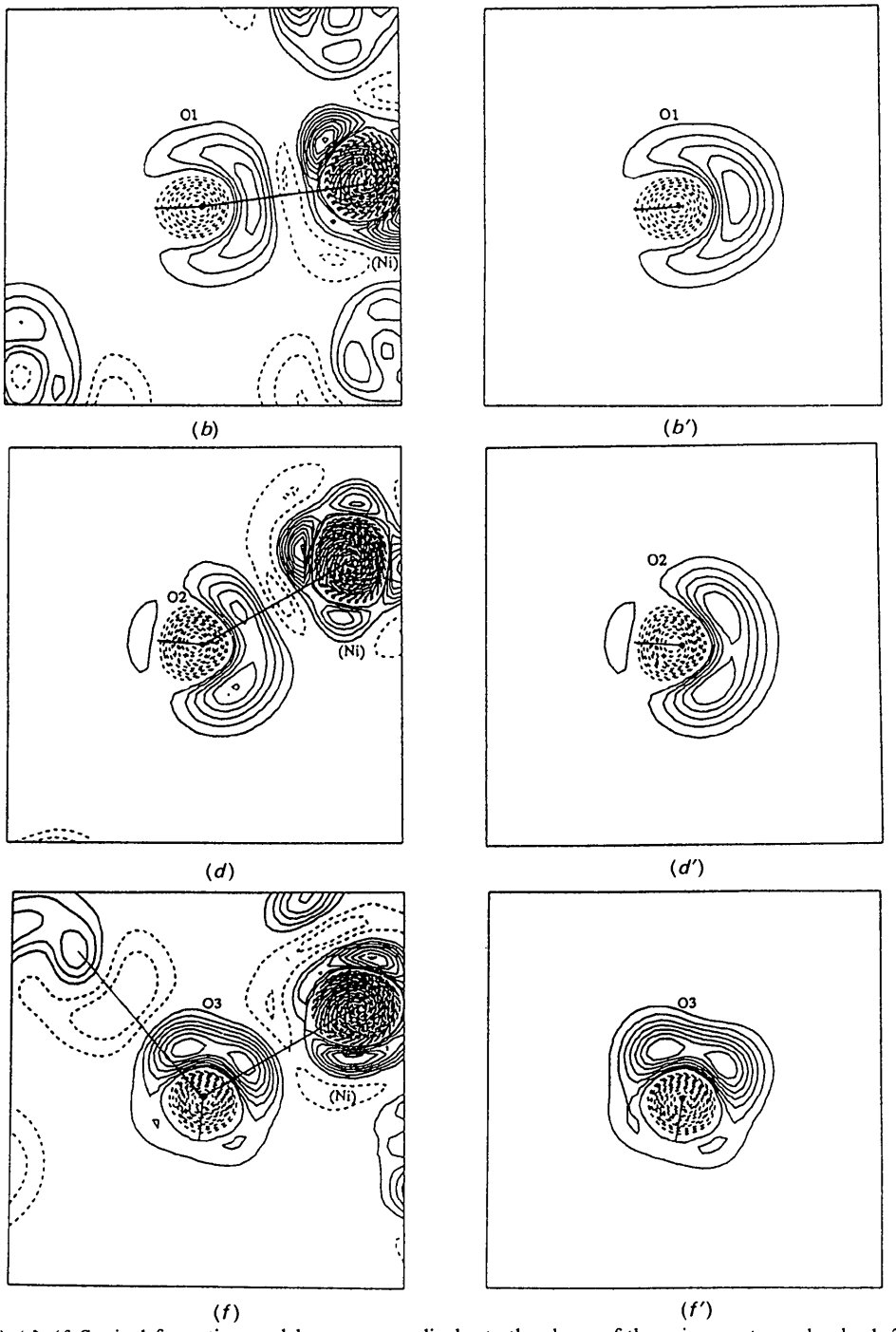

Fig. 3. (*cont.*) (*b*), (*d*), (*f*) Static deformation model maps perpendicular to the planes of the unique water molecules 1, 2, 3, respectively.

centred on a particular atom or group of atoms in a molecule, appear to remove the effect of superposition and may permit a study of the true deformations due to chemical bonding. The lone-pair regions of the three independent water molecules thus exhibit different distortions, which may be attributed to the different modes of coordination (probably predominantly a polarization effect). For a more detailed discussion of the superposition and bonding effects the recent paper by Olovsson, Ptasiewicz-Bak & McIntyre (1993) should be consulted.

If the thermal smearing is correctly deconvoluted we expect that the bonding features should be very similar at RT and 25 K since the bond distances and

angles at the two temperatures are virtually identical. This is true for the water molecules. The Ni deformation, on the other hand, is different in detail at the two temperatures, with notably more pronounced outer negative lobes and decreased positive lobes as well as a decreased inner negative lobe as the temperature increases from 25 K to RT. In view of our earlier comparison of the displacement parameters, these differences cannot be attributed to incorrect thermal deconvolution. Are the differences significant? A fit to the 25 K data with the RT deformation model gave agreement indices $R(F^2) = 0.031$, $wR(F^2) = 0.050$, $S = 1.86$; a fit to the RT data with the 25 K model gave $R(F^2) = 0.023$, $wR(F^2) = 0.040$, $S = 2.69$, in both cases a significant degradation in the fit.

The above differences in the negative and positive lobes around Ni at 25 K and RT are thus real and we postulate that they are due to differences in the relative occupancies of the energy levels at the two temperatures. From magnetic susceptibility measurements, the energy difference between the two upper partially occupied electronic levels, whatever they might be, is 4 cm^{-1} (Watanabe, 1962). From Boltzmann statistics the fraction of electrons that will remain in the lower of these levels when the temperature is increased from 25 to 300 K is 0.74, a fraction significantly different from 1.0. Since equal occupation of all 3*d* energy levels would give a spherical distribution, the major part of the aspherical density is due to the difference between the two upper levels and the three (assumed) fully occupied lower levels. Clearly, transfer of 25% of the electrons originally in the lower of the two upper levels to the higher level will cause an observable change in the aspherical

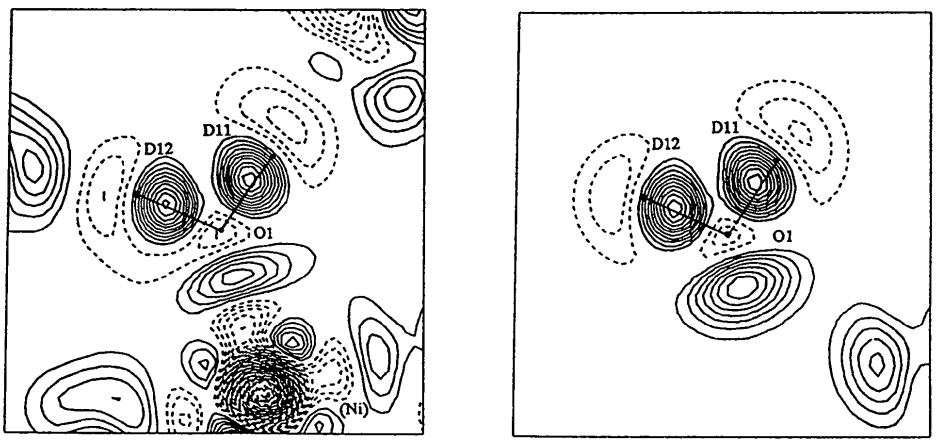

(*a*) (*a'*)

Fig. 4. Maps corresponding to Figs. 3(*a*) and 3(*a'*), based on the RT study of $NiSO_4.6D_2O$ (see caption to Fig. 2).

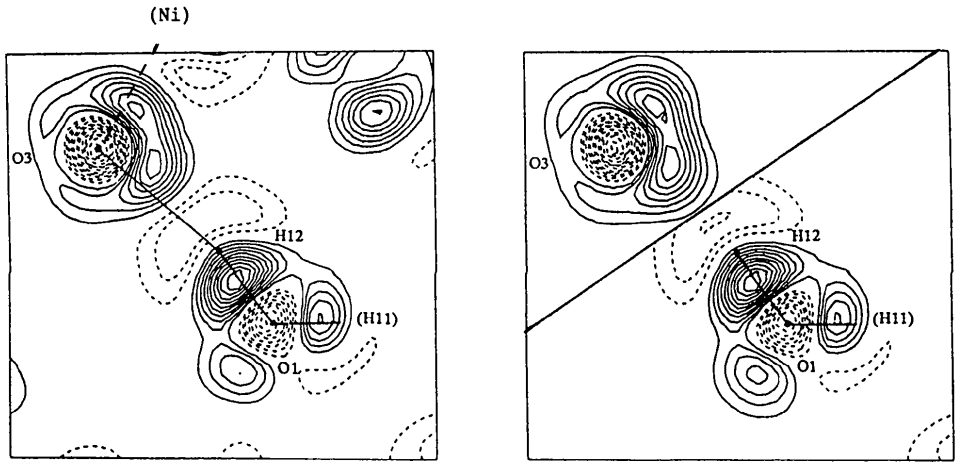

(*a*) (*a'*)

Fig. 5. Static deformation map through O(1)—H(12)···O(3). (*a*) All atoms are included in the calculation. (*a'*) Composite of the two maps with only the deformation functions of the atoms $H_2O(1)$ included in the calculation of the region near $H_2O(1)$ and only the deformation functions of O(3) included in the calculation of the region near O(3). The heavy line shows the limit of region. Reflection limit and contours as in Fig. 1.

density. Such a temperature effect would only be noticeable for elements with closely spaced partially occupied energy levels, like the 3*d* metals, but not for first- to third-row elements. This is consistent with the observation that the water densities are virtually identical at the two temperatures. If the above interpretation is correct it is, to our knowledge, the first time a temperature effect in the occupation of the electronic energy levels has been detected by diffraction methods. This effect will be further studied quantitatively by refinement of the occupation factors of the energy levels at 25 K and RT.

This work has been funded in part by the Swedish Natural Science Research Council (NFR). We gratefully acknowledge the skilful technical assistance of Mr H. Karlsson in collecting the X-ray data. We thank the ILL for allowing us access to their excellent facilities.

References

ANGEL, R. J. & FINGER, L. W. (1988). *Acta Cryst.* C**44**, 1869–1873.
BECKER, P. & COPPENS, P. (1974). *Acta Cryst.* A**30**, 129–147.
BECKER, P. & COPPENS, P. (1975). *Acta Cryst.* A**31**, 417–425.
BEEVERS, C. A. & LIPSON, H. (1932). *Z. Kristallogr.* **83**, 123–135.
CROMER, D. T. & LIBERMAN, D. (1970). *J. Chem. Phys.* **53**, 1891–1898.
CROMER, D. T. & MANN, J. B. (1968). *Acta Cryst.* A**24**, 321–324.
DOYLE, P. A. & TURNER, P. S. (1968). *Acta Cryst.* A**24**, 390–399.
ERIKSSON, A. & HERMANSSON, K. (1983). *Acta Cryst.* B**39**, 703–711.
HAREL, M. & HIRSHFELD, F. L. (1975). *Acta Cryst.* B**31**, 162–172.
HIRSHFELD, F. L. (1971). *Acta Cryst.* B**27**, 769–781.
HIRSHFELD, F. L. (1976). *Acta Cryst.* A**32**, 239–244.
HIRSHFELD, F. L. (1977). *Isr. J. Chem.* **16**, 226–229.
KUCHITSU, K. & BARTELL, L. S. (1962). *J. Chem. Phys.* **36**, 2460–2469.
LEHMANN, M. S. & LARSEN, F. K. (1974). *Acta Cryst.* A**30**, 580–584.
LUNDGREN, J.-O. (1982). *Crystallographic Computer Programs.* Report UUIC-B-13-04-05. Institute of Chemistry, Univ. of Uppsala, Sweden.
MCINTYRE, G. J., PTASIEWICZ-BAK, H. & OLOVSSON, I. (1990). *Acta Cryst.* B**46**, 27–39.
OLOVSSON, I. & JÖNSSON, P. G. (1976). *The Hydrogen Bond. Recent Developments in Theory and Experiments*, edited by P. SCHUSTER, G. ZUNDEL & C. SANDORFY, pp. 393–456. Amsterdam: North-Holland.
OLOVSSON, I., PTASIEWICZ-BAK, H. & MCINTYRE, G. J. (1993). *Z. Naturforsch. Teil A.* In the press.
SAMSON, S., GOLDISH, E. & DICK, C. F. (1980). *J. Appl. Cryst.* **13**, 425–432.
SEARS, V. F. (1986). *Methods of Experimental Physics*, Vol. 23A, *Neutron Scattering*, edited by K. SKÖLD & D. L. PRICE, pp. 521–550. New York: Academic Press.
STADNICKA, K., GLAZER, A. M. & KORALEWSKI, M. (1987). *Acta Cryst.* B**43**, 319–324.
WATANABE, T. (1962). *J. Phys. Soc. Jpn*, **17**, 1856–1864.
YAMABE, S. & MOROKUMA, K. (1975). *J. Am. Chem. Soc.* **97**, 4458–4465.

Acta Cryst. (1993). B**49**, 201–203

Structure Refinement of Mg_2Cu and a Comparison of the Mg_2Cu, Mg_2Ni and Al_2Cu Structure Types

BY F. GINGL, P. SELVAM AND K. YVON

Laboratoire de Cristallographie, Université de Genève, 24 Quai Ernest Ansermet, CH-1211 Genève 4, Switzerland

(*Received* 15 *October* 1991; *accepted* 12 *August* 1992)

Abstract

Dimagnesium copper, Mg_2Cu, $M_r = 112.170$, orthorhombic, *Fddd* (70), $a = 5.275$ (1), $b = 9.044$ (1), $c = 18.328$ (2) Å, $V = 874.3$ (2) Å^3, $Z = 16$, $D_x = 3.41$ g cm^{-3}, Mo $K\alpha$ ($\lambda = 0.71073$ Å), $\mu = 101.145$ cm^{-1}, $F(000) = 848$, $T = 293$ K, $R = 0.034$ ($wR = 0.031$) for 17 refined parameters and 310 observed X-ray single-crystal reflections [$F_o > 3\sigma(F_o)$]. The refined parameters are consistent with the nonrefined parameters reported by Schubert & Anderko [*Z. Metallkd.* (1951), **42**, 321–325]. The Mg_2Cu structure type can be derived by a stacking of slabs that build up the Al_2Cu and Mg_2Ni structure types.

0108-7681/93/020201-03$06.00

Introduction

Magnesium-rich transition-metal alloys are of interest for hydrogen-storage applications (Schlapbach, 1988). Copper-based Mg_2Cu is one of these compounds, although it has not yet been found to form a stable ternary hydride under ambient conditions (Reilly & Wiswall, 1967). Its orthorhombic structure was determined by Ekwall & Westgren (1940) and later by Schubert & Anderko (1951) but the atomic parameters stated were not refined. In this paper we report atomic parameters as refined from single-crystal X-ray diffraction and discuss the structural relationship between the Mg_2Cu, Mg_2Ni and Al_2Cu structure types.